Nonlin. Processes Geophys. Discuss., 1, 269–315, 2014
www.nonlin-processes-geophys-discuss.net/1/269/2014/
doi:10.5194/npgd-1-269-2014

Nonlinear Processes in Geophysics
Open Access
Discussions

Incidence and reflection of internal waves and wave-induced currents at a jump in buoyancy frequency

J. P. McHugh

University of New Hampshire, Durham, NH, USA

Received: 13 February 2014 – Accepted: 5 March 2014 – Published: 21 March 2014

Correspondence to: J. P. McHugh (john.mchugh@unh.edu)

Published by Copernicus Publications on behalf of the European Geosciences Union & American Geophysical Union.

Abstract

Weakly nonlinear internal gravity waves are treated in a two-layer fluid with a set of nonlinear Schrodinger equations. The layers have a sharp interface with a jump in buoyance frequency approximately modelling the tropopause. The waves are periodic in the horizontal but modulated in the vertical and Boussinesq flow is assumed. The equation governing the incident wave packet is directly coupled to the equation for the reflected packet, while the equation governing transmitted waves is only coupled at the interface. Solutions are obtained numerically. The results indicate that the waves create a mean flow that is strong near and underneath the interface, and discontinuous at the interface. Furthermore, the mean flow has an oscillatory component with a vertical wavelength that decreases as the wave packet interacts with the interface.

1 Introduction

Earth's tropopause often has a simple vertical structure with a very sudden change in the lapse rate with increasing altitude, and a corresponding sudden increase in the buoyancy frequency N. This sudden increase in N can restrict upwardly propagating internal waves, as has been known for some time (Scorer, 1949). Observations of flow in the vicinity of the tropopause has also shown unusual dynamic behavior including high turbulence levels (Partl, 1962; Worthington, 1998; Wolff and Sharman, 2008; McHugh et al., 2008b) and large wave amplitudes (McHugh et al., 2008a; Smith et al., 2008). Turbulence and waves at these altitudes is an important aspect of weather and climate, and a serious hazard to aircraft.

McHugh (2008, 2009) considered horizontally periodic internal waves interacting with an idealized model of the tropopause. The waves in McHugh (2009) were uniform while the waves in McHugh (2008) were confined to a vertical packet and treated with numerical simulations. The results indicate that while nonlinear effects are stronger near the interface even with uniform waves, a modulated amplitude results in a localized

NPGD
1, 269–315, 2014

jet-like mean flow near the interface that can be strong enough to form a critical layer, with important consequeces for later waves.

Recently Grimshaw and McHugh (2013) treated weakly nonlinear two-layer horizontally periodic waves for both unsteady and steady flow. They show expressions for the wave-induced mean flow in both layers and show that this mean flow will be discontinuous at the interface, even when the waves have evolved into a steady flow. The same two-layer flow is treated here, now including the temporal evolution.

The results here are related to previous work by Acheson (1976) and Grimshaw (1979) on over-reflection. In particular, Grimshaw (1979) considered a two layer Helmholtz velocity profile in a continuously stratified fluid with constant N throughout (no tropopause). The interface in Grimshaw (1979) is the position where the background velocity changes abruptly. Over-reflection occurs when waves that are reflected at this interface have a higher amplitude than the incident waves, while resonant over-reflection means that the incident waves are unnecessary, and the "reflected" waves are generated spontaneously by the mean flow. Grimshaw's amplitude equations assumed a balance that includes only these spontaneous modes: incident waves were relegated to higher order. The present work considers an interface with different values of N (the background mean flow is zero), and over-reflection does not exist. The balance struck here is between the incident, reflected, and transmitted waves.

Another related configuration is a layer with constant N (no interface), treated theoretically by Grimshaw (1975), Shrira (1981), Voronovich (1982), Sutherland (2006), and Tabaei and Akylas (2007). Grimshaw (1975) considered waves with a background shear flow using the wave action equation. Shrira (1981) treated weakly nonlinear waves in three dimensions assuming the modulation is the same in all directions. He derives the nonlinear Schrodinger equation that governs the wave packet evolution. Voronovich (1982) also treats weakly nonlinear waves but restricts attention to the special case with the modulation along a fixed direction. The weakly nonlinear waves in Sutherland (2006) are horizontally periodic with the modulation only in the vertical.

NPGD
1, 269–315, 2014

Tabaei and Akylas (2007) treat weakly nonlinear and finite amplitude theory with several different configurations for the modulation. Associated numerical simulations with constant N were performed by Sutherland (2001) in two dimensions.

Internal waves with no background shear will experience a modulational instability, as discussed by Whitham (1974). Wave packets propagating at a steep angle to the horizontal will focus energy, while those propagating at a shallow angle will defocus. For the waves treated here, this modulational instability may be important, depending on the wavenumbers and on the distance from the wave source to the interface. However for intermediate propagation angles, the modulational instability is too slow, and the waves interact with the interface before experiencing any significant effects.

The incident waves treated here are partially reflected at the interface, resulting in incident, reflected, and transmitted wave packets that are governed by coupled nonlinear Schrodinger (NLS) equations. Similar coupled NLS equations have been treated previously by Knobloch and Gibboon (1991) and Griffiths et al. (2006) starting with model equations such as the Klein-Gordon equation and groups of arbitrarily defined incident waves. The amplitude equations are similar to the equations given below.

The stability of plane monochromatic internal waves propagating at an angle to the horizontal were treated by Shrira (1981) and Tabaei and Akylas (2007), who showed that nonlinearity can lead to instability. Indeed Tabaei and Akylas (2007) show that the incident waves treated here are unstable for shallow angles. However the growth rate of the instability is second-order in the nonlinearity parameter, and hence the waves treated here will interact with the interface before this instability has time to grow significantly.

The reflection of nonlinear internal waves by a sloping bottom has been treated by several authors, for example Thorpe (1987) treats uniform wave trains and Tabaei et al. (2005) treat wave beams. The results show that the first few higher harmonics reflect at different angles than the primary harmonic while higher harmonics are evanescent, similar to waves reflecting from the interface treated in McHugh (2009). The mean flow

NPGD
1, 269–315, 2014

in Thorpe (1987) has an oscillatory component parallel to the slope with wavenumber equal to the difference between incident and reflected wavenumbers, and this is also found here. The mean flow in Tabaei et al. (2005) is more complex as they considered wave beams, and they do not report an oscillatory component however it is likely present in their calculations. Thorpe (1987) and Tabaei et al. (2005) do not include a modulation in the wave amplitude and their results do not have the associated mean flow. The mean flow that is present in Tabaei et al. (2005) is confined to the region where incident and reflected waves overlap. This same feature is is true here only for the oscillatory part of the mean flow. Results for a rigid horizontal lid are given here at the end for comparison and show that the interface and the rigid lid have similar behavior. The rigid boundary creates a stronger mean flow due to the stronger reflected wave.

The results given below show that the incident and reflected waves combine for a short period to create a strong localised mean flow under the interface that is discontinuous at the interface, as in Grimshaw and McHugh (2013). Furthermore there is an oscillatory component of the mean flow with a vertical wavenumber that increases as the wave packet interacts with the interface. Section 2 provides the basic equations and a derivation of the nonlinear interfacial boundary conditions. Section 3 chooses the wave modes to be included. Section 4 discusses the important mean flow, and then Sect. 5 determines the amplitude equations. Results are discussed in Sect. 6, followed by conclusions.

2 Basic equations

The flow is treated as incompressible and inviscid, and attention is restricted to two-dimensions. The stratification is due to the presence of a non-diffusing quantity, and

NPGD
1, 269–315, 2014

the flow is assumed to be Boussinesq. The flow is then governed by

$$\frac{Du}{Dt} = -\frac{1}{\rho_0}\frac{\partial p}{\partial x}, \tag{1}$$

$$\frac{Dw}{Dt} = -\frac{1}{\rho_0}\frac{\partial p}{\partial z} - b, \tag{2}$$

$$\frac{\partial u}{\partial x} + \frac{\partial w}{\partial z} = 0, \tag{3}$$

$$\frac{Db}{Dt} - N^2 w = 0. \tag{4}$$

where the velocity is (u, w), the dynamic pressure is p, ρ_0 is an average (constant) density, b is the buoyancy, defined by

$$b = \frac{g(\rho - \tilde{\rho})}{\rho_0}, \tag{5}$$

$\tilde{\rho}$ is the background density, and N is the buoyancy frequency, defined by

$$N^2 = -\frac{g\tilde{\rho}_z}{\rho_0}. \tag{6}$$

The base state must satisfy the equation of static equilibrium,

$$\frac{\partial \tilde{p}}{\partial z} = -\tilde{\rho}g, \tag{7}$$

where $\tilde{p}$ is the background pressure. The lower and upper layers have buoyancy frequency N_1 and N_2, respectively.

The kinematic condition on the interface between the layers is

$$\eta_t + u\eta_x = w, \tag{8}$$

NPGD
1, 269–315, 2014

which holds on the interface $z = \eta$, where η is the vertical displacement of the interface. Expand in a Taylor series in the same manner usually used for free surface flow:

$$\eta_t + \left[u + u_z\eta + \frac{1}{2}u_{zz}\eta^2 + \dots\right]\eta_x = \left[w + w_z\eta + \frac{1}{2}w_{zz}\eta^2 + \dots\right], \tag{9}$$

now on $z = 0$.

The dynamic condition is continuity of total pressure p_T across the interface. The total pressure is segmented into two parts:

$$p_T = \tilde{p} + p. \tag{10}$$

As the pressure difference along the interface is zero, the direction derivative of the pressure difference along this interface is also zero. This directional derivative may be written as

$$\frac{\partial}{\partial x} + \eta_x\frac{\partial}{\partial z}, \tag{11}$$

which results in

$$\left[\left(\frac{\partial}{\partial x} + \eta_x\frac{\partial}{\partial z}\right)p + \eta_x\tilde{p}_z\right]_-^+ = 0 \tag{12}$$

on $z = \eta$. The equations of motion may now be used to eliminate the derivatives of the dynamic pressure, giving

$$\left[\left(u_t + (uu)_x + (wu)_z\right) + \eta_x\left(w_t + (uw)_x + (ww)_z + b\right) + \eta_x\frac{1}{\rho_0}\tilde{p}_z\right]_-^+ = 0 \tag{13}$$

on $z = \eta$. A Taylor series is used as before, leading to

$$\left(1 + \eta\frac{\partial}{\partial z} + \dots\right)\left[\left(u_t + (uu)_x + (wu)_z\right) + \eta_x\left(w_t + (uw)_x + (ww)_z + b\right)\right]_-^+$$
$$- \eta_x\left[\eta N^2 - \frac{\eta^2}{2!}\frac{\mathrm{d}}{\mathrm{d}z}\left(N^2\right) + \frac{\eta^3}{3!}\frac{d^2}{dz^2}\left(N^2\right) + \cdots\right]_-^+ = 0 \tag{14}$$

NPGD
1, 269–315, 2014

on $z = 0$.

3 A vertically modulated wavetrain

The waves are horizontally period but modulated vertically. Define the following variables:

$$\begin{aligned} \xi &= x - c_p t, \\ \zeta &= \epsilon z, \\ \tau &= \epsilon t, \end{aligned} \tag{15}$$

where ϵ is small and measures the vertical packet length, and c_p is the horizontal phase speed.

The linear solution for a wave with upward group velocity is

$$w = \alpha I(\tau, \zeta) e^{i(k\xi - n_1 z)} + \text{cc}, \tag{16}$$

where k, n_1 are the horizontal and vertical wavenumbers, and

$$c_p^2 = \frac{N_1^2}{k^2 + n_1^2}. \tag{17}$$

Here α is small and measures the strength of the vertical velocity, and cc means complex conjugate.

When an interface is included, the solution in the lower layer requires the addition of reflected waves:

$$\alpha R(\tau, \zeta) e^{i(k\xi + n_1 z)} + \text{cc}. \tag{18}$$

Higher harmonics are expected in a Boussinesq fluid with constant N (no interface) only as a result of the modulation, and these harmonics can be made weaker by

NPGD
1, 269–315, 2014

choosing a slower modulation. The higher harmonics are $\mathcal{O}(\epsilon\alpha^2)$ and need not be included.

Further higher harmonics are generated by nonlinear effects at the interface, as shown previously by McHugh (2009). The modulation of the wavetrain does not exert the dominant influence on these interfacial harmonics, and in fact they occur even when the wave amplitude is constant (no wave packet). Hence these interfacial harmonics cannot be weakened by a slow modulation of the wave packet. However the vertical wavenumber of the interfacial harmonics is not commensurate with the primary harmonic. Hence these interface harmonics do not contribute to the evolution of the primary waves and also need not be included.

Combining all leading order contributions results in

$$w = \alpha I e^{i(k\xi - n_1 z)} + \alpha R e^{i(k\xi + n_1 z)} + \text{cc}, \quad z < 0. \tag{19}$$

The corresponding solution for the upper layer is

$$w = \alpha T(\tau, \zeta) e^{i(k\xi - n_2 z)} + \text{cc}, \quad z > 0. \tag{20}$$

The vertical wavenumber is n_2, determined to first-order by choosing the same k and frequency σ for the two layers:

$$\sigma = \frac{kN_1}{\sqrt{k^2 + n_1^2}} = \frac{kN_2}{\sqrt{k^2 + n_2^2}}. \tag{21}$$

The linear interfacial conditions result in a relationship between the amplitudes of the incident, reflected, and transmitted wave packets at the interface:

$$R = \mathcal{R} I, \tag{22}$$

$$T = \mathcal{T} I, \tag{23}$$

NPGD
1, 269–315, 2014

on $z = 0$, where

$$\mathcal{R} = \frac{n_1 - n_2}{n_1 + n_2}, \tag{24}$$

$$\mathcal{T} = \frac{2n_1}{n_1 + n_2}, \tag{25}$$

are the reflection and transmission coefficients, respectively.

4 The mean flow

Separate all dynamic fields into a ξ-averaged mean and a fluctuating part:

$$(u, w, p, b) = \left(\bar{u} + \alpha\hat{u},\ \bar{w} + \alpha\hat{w},\ \bar{p} + \alpha\hat{p},\ \bar{b} + \alpha\hat{b}\right), \tag{26}$$

where the bar indicates mean, e.g. $\bar{u}$, and the hat indicates the fluctuating part, composed of all wave components. The ξ-average will also be indicated with $< \cdot >$. Only the horizontal mean flow $\bar{u}$ is needed for the final amplitude equations.

Following Acheson (1976), Scinocca and Shepherd (1992), and Grimshaw and McHugh (2013), an explicit expression for $\bar{u}$ can be found. Introduce the vorticity χ:

$$\chi = u_z - w_x, \tag{27}$$

$$\chi_t + (u\chi)_x + (w\chi)_z = b_x. \tag{28}$$

Include Eq. (15):

$$\chi = u_z + \epsilon u_\zeta - w_\xi, \tag{29}$$

$$-c_p\chi_\xi + \epsilon\chi_\tau + (u\chi)_\xi + (w\chi)_z + \epsilon(w\chi)_\zeta = b_\xi. \tag{30}$$

Average Eqs. (29) and (30), combine, and scale as above to obtain

$$\epsilon\bar{u}_{z\tau} + \epsilon^2\bar{u}_{\zeta\tau} + \alpha^2 < \hat{w}\hat{\chi} >_z + \epsilon\alpha^2 < \hat{w}\hat{\chi} >_\zeta = 0. \tag{31}$$

NPGD
1, 269–315, 2014

Scale the horizontal mean flow using

$$\bar{u} \rightarrow \alpha_0 \bar{u}, \tag{32}$$

where the relationship between α_0 and α, ϵ needs to be determined. To leading order,

$$\epsilon \alpha_0 \bar{u}_{z\tau} + \alpha^2 < \hat{w}\hat{\chi} >_z \approx 0, \tag{33}$$

which may be integrated to produce

$$\epsilon \alpha_0 \bar{u}_\tau + \alpha^2 < \hat{w}\hat{\chi} > \approx 0. \tag{34}$$

Furthermore, it may be shown using $N^2 \hat{w} \approx -c_p \hat{b}_\xi + \epsilon \hat{b}_\tau$ and $\hat{b}_\xi \approx -c_p \hat{\chi}_\xi + \epsilon \hat{\chi}_\tau$ that

$$< \hat{w}\hat{\chi} > \approx \epsilon \frac{1}{N^2} < \hat{b}\hat{\chi} >_\tau, \tag{35}$$

causing Eq. (34) to become

$$\alpha_0 \bar{u}_\tau + \alpha^2 \frac{1}{N^2} < \left(\hat{b}\hat{\chi}\right) >_\tau \approx 0. \tag{36}$$

At this point it may be seen that in order for this equation to balance, the horizontal mean flow must scale according to

$$\alpha_0 = \alpha^2. \tag{37}$$

Integrate Eq. (36) and use $\hat{b} \approx -c_p \hat{\chi}$ in the bracketed term to achieve

$$\bar{u} = \frac{1}{c_p N^2} < \hat{b}^2 > . \tag{38}$$

NPGD
1, 269–315, 2014

Finally, the mean flow in the lower layer is

$$\bar{u} = \bar{u}_{\mathrm{m}} + \left(\bar{u}_i e^{i2n^- z} + \bar{u}_i^* e^{-i2n^- z}\right),\ z < 0, \tag{39}$$

where

$$\bar{u}_{\mathrm{m}} = \frac{2}{c_{\mathrm{p}}}\frac{N_1^2}{\sigma^2}\left(II^* + RR^*\right), \tag{40}$$

$$\bar{u}_i = \frac{2}{c_{\mathrm{p}}}\frac{N_1^2}{\sigma^2} I^* R. \tag{41}$$

There are two parts to this mean flow. One part is $\bar{u}_{\mathrm{m}}$, which is identical to the mean flow that would be obtained if the incident and reflected wave packets were acting individually, and the mean flows are merely added. The second part is the term containing $\bar{u}_i$, which is caused by the interference between the incident and reflected waves.

In the upper layer,

$$\bar{u} = \frac{2}{c_{\mathrm{p}}}\frac{N_2^2}{\sigma^2} TT^*,\ z > 0. \tag{42}$$

5 The interaction equations

The leading order contributions to the primary harmonic in Eqs. (1)–(4) will arise from linear terms and from interactions between the wave perturbations and the mean flow, as in Tabaei and Akylas (2007). Hence the leading-order primary-harmonic terms in

NPGD
1, 269–315, 2014

Eqs. (1)–(4) are

$$-c_{\mathrm{p}}\hat{u}_{\xi} + \epsilon\hat{u}_{\tau} + \alpha^2\bar{u}\hat{u}_{\xi} + \alpha^2\bar{u}_z\hat{w} = -\frac{1}{\rho_0}\hat{p}_{\xi}, \tag{43}$$

$$-c_{\mathrm{p}}\hat{w}_{\xi} + \epsilon\hat{w}_{\tau} + \alpha^2\bar{u}\hat{w}_{\xi} = -\frac{1}{\rho_0}\left(\hat{p}_z + \epsilon\hat{p}_{\zeta}\right) - \hat{b}, \tag{44}$$

$$\hat{u}_{\xi} + \hat{w}_z + \epsilon\hat{w}_{\zeta} = 0 \tag{45}$$

$$-c_{\mathrm{p}}\hat{b}_{\xi} + \epsilon\hat{b}_{\tau} + \alpha^2\bar{u}\hat{b}_{\xi} - N^2\hat{w} = 0. \tag{46}$$

Using Eqs. (19) and (20), and similar expressions for the other variables in Eqs. (43)–(46) and keeping only terms that contribute to the primary harmonic at the leading order results in a separate set of equations for the incident, reflected, and transmitted wavetrains. For the incident waves the resulting equation is

$$\left[D_t D_z D_t D_z - k^2\left(D_t^2 + N_1^2\right)\right]I - \alpha^2 2\sigma\left[(k^2 + n_1^2)k\bar{u}_m I + (k^2 - n_1^2)k\bar{u}_i^* R\right] = 0, z < 0, \tag{47}$$

where

$$D_t = \epsilon\frac{\partial}{\partial\tau} - i\sigma, \tag{48}$$

$$D_z = \epsilon\frac{\partial}{\partial\zeta} - in_1. \tag{49}$$

If $\epsilon = \alpha$, then a simpler form is achieved:

$$I_{\tau} + c_{\mathrm{g}}I_{\zeta} - i\epsilon\frac{1}{2}c_{\mathrm{g}}'I_{\zeta\zeta} + i\epsilon\frac{2}{\sigma}\left[\left(k^2 + n_1^2\right)\left(|I|^2 + |R|^2\right) + \left(k^2 - n_1^2\right)|R|^2\right]I = 0, \quad z < 0, \tag{50}$$

where c_{g} is the vertical group velocity,

$$c_{\mathrm{g}} = \sigma\frac{n_1}{k^2 + n_1^2}, \; z < 0, \tag{51}$$

NPGD
1, 269–315, 2014

and c_g' is a derivative of the group velocity:

$$c_g' = \frac{\partial c_g}{\partial n_1} = \sigma \frac{k^2 - 2n_1^2}{\left(k^2 + n_1^2\right)^2}, \; z < 0. \tag{52}$$

A similar development for the reflected and transmitted waves leads to

$$R_\tau - c_g R_\zeta - i\epsilon \frac{1}{2} c_g' R_{\zeta\zeta} + i\epsilon \frac{2}{\sigma} \left[\left(k^2 + n_1^2\right) \left(|I|^2 + |R|^2\right) + \left(k^2 - n_1^2\right) |I|^2 \right] R = 0, \;\; z < 0, \tag{53}$$

$$T_\tau + c_g T_\zeta - i\epsilon \frac{1}{2} c_g' T_{\zeta\zeta} + i\epsilon \frac{2}{\sigma} \left(k^2 + n_2^2\right) |T|^2 T = 0, \;\; z > 0, \tag{54}$$

where

$$c_g = \sigma \frac{n_2}{k^2 + n_2^2}, \;\; z > 0, \tag{55}$$

and

$$c_g' = \frac{\partial c_g}{\partial n_2} = \sigma \frac{k^2 - 2n_2^2}{\left(k^2 + n_2^2\right)^2}, \;\; z > 0. \tag{56}$$

The interfacial conditions must be treated in the same manner. Keeping only quadratic terms,

$$\eta_t + (u\eta)_x = w, \tag{57}$$

$$\left[u_t + (uu)_x + (uw)_z + \eta_x w_t + \eta u_{zt} + \eta_x b - N^2 \eta \eta_x \right]_-^+ = 0, \tag{58}$$

NPGD
1, 269–315, 2014

on $z = 0$. Using (15), these are

$$-c_p\eta_\xi + \epsilon\eta_\tau + (u\eta)_\xi = w, \tag{59}$$

$$\left[-c_p u_\xi + \epsilon u_\tau + (uu)_\xi + (uw)_z + \epsilon(uw)_\zeta - c_p\eta_\xi w_\xi + \epsilon\eta_\xi w_\tau - c_p\eta u_{z\xi} + \epsilon\eta u_{z\tau} - \epsilon c_p\eta u_{\zeta\xi} + \eta_\xi b - N^2\eta\eta_\xi\right]_-^+ = 0, \tag{60}$$

on $z = 0$, where higher-order terms have again been deleted. Using Eq. (26) and keeping only terms that contribute to the first harmonic gives

$$-c_p\hat{\eta}_\xi + \epsilon\hat{\eta}_\tau + \alpha^2\bar{u}\hat{\eta}_\xi = \hat{w}, \tag{61}$$

$$\left[-c_p\hat{u}_\xi + \epsilon\hat{u}_\tau + \alpha^2\bar{u}\hat{u}_\xi\right]_-^+ = 0, \tag{62}$$

on $z = 0$, after some simplification. Insert Eqs. (19) and (20) along with associated expressions for the horizontal component of velocity into Eqs. (61) and (62) and simplify to achieve a relationship between the reflected and transmitted wave amplitudes R, T and the incident wave amplitude I at the interface:

$$R + \epsilon\frac{i}{\sigma}R_\tau = \left[\frac{n_1 - n_2}{n_1 + n_2}\right]\left[I + \epsilon\frac{i}{\sigma}I_\tau\right] + \mathcal{O}(\alpha^2), \tag{63}$$

$$T + \epsilon\frac{i}{\sigma}T_\tau = \left[\frac{2n_1}{n_1 + n_2}\right]\left[I + \epsilon\frac{i}{\sigma}I_\tau\right] + \mathcal{O}(\alpha^2) \tag{64}$$

on $z = 0$. Hence nonlinear effects in the interfacial conditions are $\mathcal{O}(\alpha^2)$, which is two orders different from the leading order term in Eqs. (63) and (64), and therefore higher order (as in Eq. 50, where terms $\mathcal{O}(\alpha^2)$ are deleted). Hence the nonlinear effects in the interfacial conditions may be neglected with the present theory. The remaining terms in the interfacial conditions are balanced with the linear conditions,

$$R = \mathcal{R}I, \tag{65}$$

$$T = \mathcal{T}I, \tag{66}$$

NPGD
1, 269–315, 2014

on $z = 0$. Note that these conditions imply continuity of velocity of the wave components. Importantly the *total* velocity is not necessarily equal at the interface as the mean flow may not be continuous.

6 Results

The amplitude equations (50), (53), and (54) are solved here numerically. Spatial derivatives are evaluated with second-order central differences. Temporal integration is achieved with the fourth-order Adams-Bashforth method, resulting in explicit algebraic equations (see Ames, 1977 for a general discussion). The boundary point at the end of the domain is treated with the second-order upwind scheme. This one-sided method allows waves to exit the region without significant reflections (the reflected waves have already been treated in the derivation of the amplitude equations).

All variables are rescaled with the horizontal wavenumber k and the buoyancy frequency in the lower layer N_1. The buoyancy frequency ratio for two-layer cases is chosen to have the value $N_2/N_1 = 2$, matching approximately Earth's tropopause. The results then depend on two parameters: ϵ and n_1/k. The parameter ϵ measures the wave packet length and appears as a simple coefficient of both the dispersion and nonlinear terms in all amplitude equations. This relatively simple dependence on ϵ suggests that the waves evolve with the scales $\epsilon^2 t$ and $\epsilon^2 z$, and indeed the parameter ϵ disappears if these scales are introduced. Hence a larger value of ϵ merely results in a faster evolution of the wave packet with no other differences. However ϵ is retained here to make the computations more practical. The value of ϵ is set by the choice of the number of waves in the wave packet, chosen here to be five. This choice also sets the wave amplitude α, since $\alpha = \epsilon$.

NPGD
1, 269–315, 2014

A wave envelope is created at the bottom boundary by imposing the value of the real part of I to be the raised cosine function:

$$I = \frac{1}{2}\left[1 - \cos\frac{\tau}{Q}\right], \tag{67}$$

$\tau \in [0, Q]$, where Q is the wave period times the number of waves in the wave packet. Other wave packet shapes, such as a Gaussian shape, have been considered and produce the same general results.

The behavior with increasing n_1/k is complex. The reflection and transmission coefficients $\mathcal{R}$, $\mathcal{T}$ given by Eqs. (24) and (25) depend on n_1/k, as shown in Fig. 1. For very small values of n_1/k, $\mathcal{R}$ approaches unity while $\mathcal{T}$ approaches zero, indicating that the waves are nearly perfectly reflected. As n_1/k increases, $\mathcal{R}$ approaches the value 1/3 while $\mathcal{T}$ approaches 2/3. Hence for large values of n_1/k, the reflection and transmission coefficients are approximately constant. Perfect transmission never occurs for any value of n_1/k.

The results given below will show that the mean flow given in Eqs. (39) and (42) increases strongly with n_1/k, as measured approximately by the factor $\frac{N_1^2}{c_p\sigma^2}$. This increase is primarily due to the direction of the group velocity becoming more horizontal as n_1/k increases. After rescaling, define U to be this factor:

$$U = \frac{1}{2}\left(\frac{k^2 + n_1^2}{k^2}\right)^{3/2}. \tag{68}$$

Profiles of the mean flow velocity appearing in the figures are normalized by U.

The coefficient of the nonlinear term and the dispersion term in the amplitude equation governing the incident waves (50) are plotted in Fig. 2. The value of the nonlinear term can be seen to increase strongly with n_1/k, as a direct result of the mean flow dependence on n_1/k. Hence stronger nonlinear effects are expected as n_1/k increases.

NPGD
1, 269–315, 2014

The dispersion coefficient is negative for small values of n_1/k, and changes sign at $n_1/k = 1/\sqrt{2}$. As discussed by Whitham (1974), the waves experience a modulational instability in the region where this coefficient is negative. As a result of this instability, a wave packet will become more focused and grow in amplitude. This dispersion coefficient is positive for $n_1/k > 1/\sqrt{2}$ and reaches a maximum at $n_1/k = \sqrt{2}$. When the coefficient is positive, the wave packet defocuses.

First consider constant N throughout and let $n_1/k = 1/\sqrt{2}$. This special value of n_1/k has a zero value for the coefficient of the dispersion term, hence there are no modulational effects at this order. Figure 3 shows vertical profiles of wave amplitude and mean flow at three times. Note that a time value of zero here corresponds to the wave packet centered at the origin, which is also the mean position of the interface in two-layer cases. Each time value in Fig. 3 shows three panels, which contain (from left to right in each subfigure) a vertical profile of the wave magnitude, the wave phase, and the wave-induced mean flow. Comparing the left panel in Fig. 3a to that in Fig. 3c, it can be seen that the wave packet moves vertically without any significant change in shape. In fact, if the dispersion term is deleted from Eq. (50), then the magnitude of the incident waves would propagate with

$$|I|_\tau + c_g |I|_\zeta = 0, \tag{69}$$

confirming that the wave packet should propagate with the group velocity c_g but without the packet shape evolving. The phase ϕ under these same conditions obeys

$$\phi_\tau + c_g \phi_\zeta + \epsilon \left(k^2 + n_1^2\right) |I|^2 = 0. \tag{70}$$

Hence the phase is strongly influenced by nonlinearity, as can be seen in Fig. 3, where oscillations in phase develop as the packet ascends.

A corresponding two-layer case is shown in Fig. 4 using the same $n_1/k = 1/\sqrt{2}$ value as the above one-layer case. The Brunt–Vaisala frequency ratio is $N_2/N_1 = 2$ and the interface is at the center of each panel ($z = 0$) as indicated with a dashed line. The

NPGD
1, 269–315, 2014

three time values are chosen to correspond to (a) before the wave packet has reached the interface, (b) as the packet is transiting the interface, and (c) after the packet has passed through the interface. The dashed profiles are the magnitude and phase for the downward moving wave packet (the reflected wave), and the solid profiles are the upward moving waves (incident and transmitted waves). Note that there is only a single profile for the mean flow in the lower layer (e.g. no dashed profile) as it is due to the combination of incident and reflected waves.

Figure 4b has all three wave packets present simultaneously. The mean flow at this stage shows the very striking discontinuity at the interface. The reason for this discontinuity is that in the lower layer the mean flow is driven by both incident and reflected wave. Since they both have a horizontal component of group velocity that is positive, then the mean flow they generate is positive, despite having a vertical group velocity that has opposite sign. In contrast, the upper layer only has the transmitted wave driving a mean flow, and is therefore always weaker, even at the interface.

The mean flow in Fig. 4b shows oscillations that are not present before the packet reaches the interface or in the single layer case. These oscillations are due to the interference mean given by Eqs. (39) and (41). The interference mean only occurs *under* the mean position of the interface, and exists when the incident wave and reflected wave are overlapping and therefore is rather short-lived.

Figure 4c shows a later time, after the incident wave packet has been completed converted into reflected and transmitted wave packets. The wave-induced mean flow is now much reduced in strength as a result of the smaller amplitude of both transmitted and reflected waves, as compared to the incident wave in Fig. 4a. The reflected wave packet retains the original shape of the incident wave packet with no apparent change due to the nonlinear interaction at the interface. The coefficient of dispersion in the upper layer is not zero, and the wave packet shape can be seen to have evolved somewhat in Fig. 4c.

A close-up view of the wave amplitude as the wave packet is transiting the interface is shown in Fig. 5 for a sequence of time values, each profile shifted by a value of

NPGD
1, 269–315, 2014

1.5 for display. Note that the disturbance velocity in this model is continuous, even though it appears to be discontinuous in Fig. 5. Figure 6 shows corresponding profiles of the mean flow, which is indeed discontinuous at the interface during this period. The discontinuity is formed by the 'front' of the wave packet and would then be maintained until the 'back' of the wave packet terminates the interfacial mean. Thus the discontinuous flow would remain if the waves evolved into a uniform field.

The coefficient of the dispersion term is negative when $n_1/k < 1/\sqrt{2}$. The evolution of the wave packet for such a case is shown in Fig. 7 for a single layer with constant N and $n_1/k = 0.4$. This same single-layer case was previously treated by Sutherland (2001) and Tabaei and Akylas (2007). Figure 7 shows that the wave amplitude and the associated mean flow are focusing energy toward the center of the wave packet. This behavior is due to the modulational instability discussed by Whitham (1974). The focusing effect continues as the packet ascends achieving very large values for I and and nearly forming a cusp, finally reaching a stage where the numerical solution fails. Note in Fig. 7 that the phase evolves in a manner very similar to the previous case (Fig. 3).

The two layer case with $n_1/k = 0.4$ is shown in Fig. 8. The focusing effect that is evident in the single-layer case has only begun to form when the wave packet reaches the interface, hence the results in Fig. 8 are very similar to the case with $n_1/k = 1/\sqrt{2}$ in Fig. 4, which has zero dispersion in the lower layer. However, contrasting Figs. 4b and 8b one can see that the interference mean flow is stronger with $n_1/k = 0.4$ as a result of dispersion. If the wave packet had evolved for a longer distance before reaching the interface, then the incident wave amplitude would be more focused and the oscillations in the mean flow would be further exaggerated.

After interacting with the interface the reflected and transmitted waves are much smaller in amplitude than the incident waves. However the tendency to focus continues in both layers, despite the smaller amplitude. The focused packet shape would not form at these parameter values without the interface. In this manner the interface allows

NPGD
1, 269–315, 2014

more complexity above the interface, even while reducing the amplitude of upwardly propagating waves.

Figures 9 and 10 show results for a case when the coefficient of dispersion is positive, $n_1/k = 1$. Figure 9 shows the wave packets in a single-layer case with constant N while Fig. 10 is the corresponding two-layer configuration with $N_2/N_1 = 2$. Figure 9 shows that as the wave packet ascends in a single layer, the packet shape tends to defocus, smoothing out the center of the packet. Note in Fig. 9 that the phase develops similar but more rapid oscillations as the previous case. The more rapid oscillations in phase are due to the stronger nonlinear effects that are present as n_1/k increases.

The two-layer results in Fig. 10b show that the mean flow is again discontinuous as the wave packet interacts with the interface, and that the interference mean is again present. Figure 10c shows that both the reflected and transmitted wave packets are significantly altered compared to the incident wave packet and the single-layer case.

One of the nonlinear terms in Eqs. (50) and (53) is directly attributed to the interference mean flow, and has the rescaled coefficient

$$1 - \frac{n_1^2}{k^2}. \tag{71}$$

If $n_1/k = 1$ then this coefficient is zero, and therefore the interference mean does not influence the evolution of the waves directly, despite $\bar{u}_j$ being nonzero. Hence $n_1/k = 1$ is a special case.

Figures 11 and 12 again show a close-up view of a sequence of profiles of the wave magnitude and corresponding mean flow as the packet transits the interface. Figure 12 shows the development of the discontinuity in the mean flow as well as the appearance of the interference mean flow. Another feature evident in Fig. 12 is that the oscillations in the mean flow under the interface are changing wavelength as time increases, something that is caused by nonlinear effects. The effect is present for previous cases but is not as prominent. This change in wavelength is due to the nonlinear interaction

NPGD
1, 269–315, 2014

between the interference mean and the oscillations in phase that continue to increase as the wave packet ascends. This effect becomes more pronounced as n_1/k increases.

Figures 13–16 show results for $n_1/k = \sqrt{2}$. This value of n_1/k corresponds to the maximum value of the dispersion coefficient in the amplitude equations for the lower layer. Figure 13 provides wave profiles for a single layer of constant N, and shows that the wave packet spreads considerably as it ascends. Figure 14 gives results for the corresponding two-layer case. For this relatively large value of n_1/k, the wave packet evolves quickly and has distorted into a rather flat profile in it's center by the time the packet reaches the interface. Figures 15 and 16 again provide a close-up of the interface region and show a process similar to the previous cases, including the discontinuous mean flow. Figure 16 shows the interference mean and the now striking change in wavenumber that occurs. This effect is now more pronounced due to the increased strength of the nonlinear effect.

Larger values of n_1/k have somewhat weaker dispersion coefficients, but significantly stronger nonlinear effects. Resolving the mean flow with larger values of n_1/k becomes very difficult due to the small scale oscillations in the interference mean.

The overall mean-flow strength near the interface is shown in Figs. 17–19 for three examples. These figures show a time evolution of the maximum of the wave packet amplitude for two-layer cases. In Fig. 17, $n_1/k = 1/\sqrt{2}$ and the dispersion is zero. For this case the maximum value of the wave amplitude is constant until the waves interact with the interface. While the packet is near the interface, the mean flow is enhanced due to the combination of the incident and reflected waves, and also the interference mean. Figure 17 shows that the mean flow is enhanced by a factor of approximately 1.75 at the peak. Figure 18 has $n_1/k = 0.4$ and shows that the maximum value is more than twice the value of the mean flow early in the simulation. Also evident here is the more gradual increase in mean that is associated with the focusing effect with negative dispersion.

Figure 19 has $n_1/k = \sqrt{2}$ where the dispersion coefficient is positive and maximum. Here the wave packet is defocusing, resulting in a decrease in the maximum value

NPGD
1, 269–315, 2014

as the wave packet ascends. The increase in mean at the interface is not strong enough to overcome this decrease, and hence the maximum value of mean flow is at the beginning of the simulation. Overall, Figs. 17–19 indicate that smaller values of n_1/k are more likely to have an enhanced jet-like mean flow under the interface.

Also shown in Figs. 17–19 is a dashed line showing the velocity difference at the interface, and a thick solid line showing the maximum of the interference mean. In each figure, these two quantities are approximately the same. However the velocity difference is not caused by the interference mean, rather they are both caused by the overlapping of the incident and reflected wave packets, and hence have approximately the same strength. Note that the velocity difference for $n_1/k = 0.4$ in Fig. 17 is stronger compared to the $n_1/k = 1/\sqrt{2}$ in Fig. 17. Figure 20 provides this maximum velocity difference for an interval of n_1/k, extracted from the simulations. This figure shows that the velocity difference is directly related to the reflection coefficient figure 1.

If the interface is replaced with a rigid lid, then the waves are completed reflected, but otherwise behave in the same manner as above. The interfacial boundary conditions are replaced with

$$w = 0 \tag{72}$$

on $z = 0$, resulting in

$$\mathcal{R} = -1,\ \mathcal{T} = 0. \tag{73}$$

The incident and reflected wave amplitudes are still governed by Eqs. (50) and (53), while the mean flow is still determined with Eq. (39).

An example case with $n_1/k = 1$ is shown in Fig. 21 with vertical profiles of wave magnitude and phase and the mean flow at three time steps, as before. Notice in Fig. 21 that the wave magnitude and mean flow when the packet is moving upward ($N_1\tau \approx -52$) have the same profile after bouncing off the rigid lid and is moving downward ($N_1\tau \approx +52$). The only difference other than the direction of propagation is the phase which is more oscillatory. The mean flow for $N_1\tau \approx 0$ is much stronger than the above case

NPGD
1, 269–315, 2014

with an interface as a result of the much stronger reflected wave. The maximum of the mean flow is now approximately three times the mean flow of the incident wave packet, compared to a factor of 1.75 in the case with the interface. The interference mean flow is still present with a rigid lid, and would be more prominent as n_1/k becomes larger.

7 Conclusions

Atmospheric observations indicate that the tropopause altitude is more likely to experience turbulence and large amplitude waves than other altitudes. The abrupt change in the buoyancy frequency suggests that such observations are related to the dynamics of internal waves near the tropopause. Previous numerical simulations conclude that internal waves will create a wave-induced jet-like mean flow in the tropopause vicinity that is likely responsible for at least some of the observations. Weakly nonlinear waves crossing an idealized tropopause are considered here, resulting in a trio of nonlinear amplitude equations.

The wave-induced mean flow is found to be greatest in the vicinity of the interface. Furthermore, this mean flow is discontinuous at the interface, and would be a region of strong shear in a viscous flow. The effects of dispersion may act to enhance this jet-like flow. The mean flow also has an oscillatory component, and vertical wavelength of the the oscillation decreases as a result of the the nonlinear interaction between the mean flow and the incident and reflected waves.

References

Acheson, D. J.: On over-reflexion, J. Fluid Mech., 77, 433–472, 1976. 271, 278
Ames, W. F.: Numerical methods for partial differential equations, Academic Press, 1977. 284
Griffiths, S. D., Grimshaw, R. H. J., and Khusnutdinova, K. R.: Modulational instability of two pairs of counter-propagating waves and energy exchancge in a two-component system, Physica D, 214, 1–24, 2006. 272

NPGD
1, 269–315, 2014

Grimshaw, R. and McHugh, J. P.: Steady and unsteady nonlinear internal waves incident on an interface, Q. J. Roy. Meteor. Soc., 139, 1990–1996, 2013. 271, 273, 278
Grimshaw, R. H. J.: Nonlinear internal gravity waves and their interaction with the mean wind, J. Atmos. Sci., 32, 1779–1793, 1975. 271
Grimshaw, R. H. J.: On resonant over-reflexion of internal gravity waves from a Helmholtz velocity profile, J. Fluid Mech., 90, 161–178, 1979. 271
Knobloch, E. and Gibbon, J. D.: Coupled NLS equations for counter propagating waves in systems with reflection symmetry, Phys. Lett. A, 154, 353–356, 1991. 272
McHugh, J. P.: Mean flow generated by an internal wave packet impinging on the interface between two layers of fluid with continuous density, Theor. Comp. Fluid Dyn., 22, 107–123, 2008. 270
McHugh, J. P.: Internal waves at an interface between two layers of differing stability, J. Atmos. Sci., 66, 1845–1855, 2009. 270, 272, 277
McHugh, J. P., Dors, I., Jumper, G. Y., Roadcap, J., Murphy, E., and Hahn, D.: Large variations in balloon ascent rate over Hawaii, J. Geophys. Res., 113, D15123, doi:10.1029/2007JD009458, 2008a. 270
McHugh, J. P., Jumper, G. Y., and Chun, M.: Balloon thermosonde measurements over Mauna Kea, and comparison with seeing measurements, Publ. Astron. Soc. Pac., 120, 1318–1324, 2008b. 270
Partl, W.: Clear air turbulence at the tropopause levels, Navigation, 9, 288–295, 1962. 270
Scinocca, J. F. and Shepherd, T. G.: Nonlinear wave-activity conservation laws and Hamiltonian structure for the two-dimensional anelastic equations, J. Atmos. Sci., 49, 5–27, 1992. 278
Scorer, R. S.: Theory of waves in the lee of mountains, Q. J. Roy. Meteor. Soc., 75, 41–56, 1949. 270
Smith, R. B., Woods, B. K., Jensen, J., Cooper, W. A., Doyle, J. D., Jiang, Q., and Grubisic, V.: Mountain waves entering the stratosphere, J. Atmos. Sci., 65, 2543–2562, 2008. 270
Shrira, V. I.: On the propagation of a three-dimensional packet of weakly non-linear internal gravity waves, Int. J. Nonlin. Mech., 16, 129–138, 1981. 271, 272
Sutherland, B. R.: Finite-amplitude internal wavepacket dispersion and breaking, J. Fluid Mech., 429, 343–380, 2001. 272, 288
Sutherland, B. R.: Weakly nonlinear internal gravity wavepackets, J. Fluid Mech., 569, 249–258, 2006. 271

NPGD
1, 269–315, 2014

Tabaei, A. and Akylas, T. R.: Resonant long-short wave interactions in an unbounded rotating stratified fluid, Stud. Appl. Math., 119, 271–296, 2007. 271, 272, 280, 288
Tabaei, A., Akylas, T. R., and Lamb, K. G.: Nonlinear effects in reflecting and colliding internal wave beams, J. Fluid Mech., 526, 217–243, 2005. 272, 273
Thorpe, S. A.: On the reflection of a train of finite-amplitude internal waves from a uniform slope, J. Fluid Mech., 178, 279–302, 1987. 272, 273
Voronovich, A. G.: On the propagation of a packet of weakly nonlinear internal waves in a medium with constant Vaisala frequency, Izv. Atmos. Ocean Phy., 18, 247–250, 1982. 271
Whitham, G.: Linear and nonlinear waves, Wiley, 1974. 272, 286, 288
Wolff, J. K. and Sharman, R. D.: Climatology of upper-level turbulence over the contiguous United States, J. Appl. Meteorol. Clim., 47, 2198–2214, 2008. 270
Worthington, R. M.: Tropopausal turbulence caused by the breaking of mountain waves, J. Atmos. Sol.-Terr. Phy., 60, 1543–1547, 1998. 270

NPGD
1, 269–315, 2014

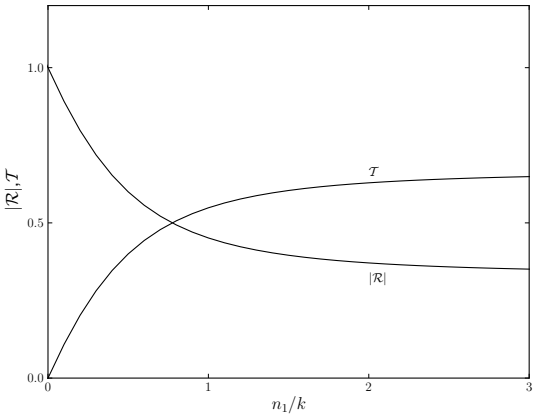

Fig. 1. Transmission coefficient $\mathcal{T}$ and absolute value of the reflection coefficient $|\mathcal{R}|$ as n_1/k increases.

NPGD
1, 269–315, 2014

Incidence and reflection of internal waves

J. P. McHugh

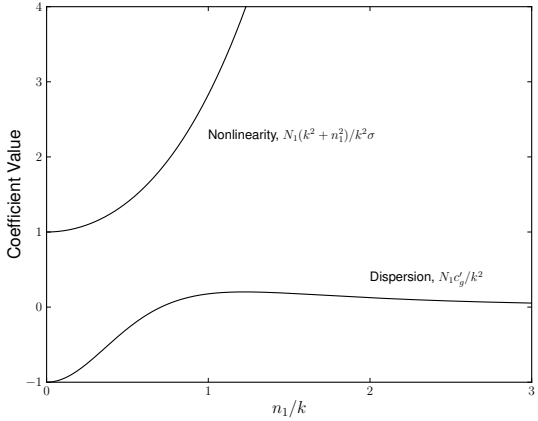

Fig. 2. Behavior of the coefficients of the dispersion and nonlinear terms in the amplitude equations as n_1/k increases.

NPGD
1, 269–315, 2014

Incidence and reflection of internal waves

J. P. McHugh

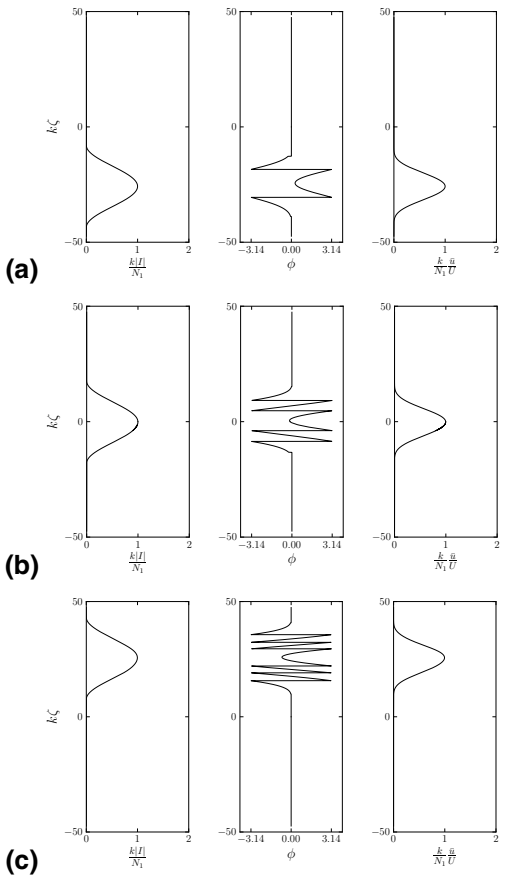

Fig. 3. Vertical profiles of the wave magnitude (left panel), phase (center panel), and mean flow (right panel) at three times in a single layer of constant N with $n_1/k = 1/\sqrt{2}$. **(a)** $N_1\tau \approx -66$, **(b)** $N_1\tau \approx 0$, and **(c)** $N_1\tau \approx +66$.

NPGD
1, 269–315, 2014

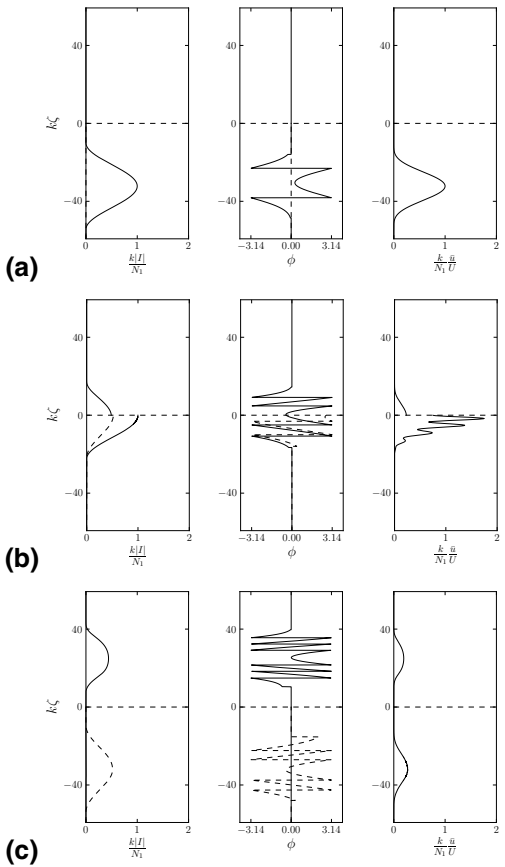

Fig. 4. Vertical profiles of the wave magnitude (left panel), phase (center panel), and mean flow (right panel) at three times in two layers. The parameter values are $n_1/k = 1/\sqrt{2}$ and $N_2/N_1 = 2$. **(a)** $N_1\tau \approx -66$, **(b)** $N_1\tau \approx 0$, and **(c)** $N_1\tau \approx +66$.

NPGD
1, 269–315, 2014

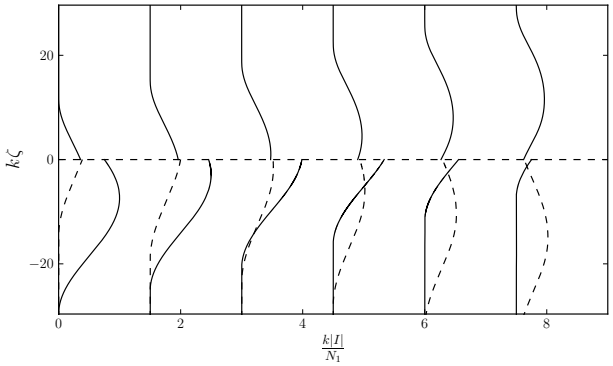

Fig. 5. Vertical profiles of the wave magnitude in two layers for a sequence of times. Each profile is shifted by a value of 1.5 for display. The parameter values are $n_1/k = 1/\sqrt{2}$, and $N_2/N_1 = 2$.

NPGD
1, 269–315, 2014

Incidence and reflection of internal waves

J. P. McHugh

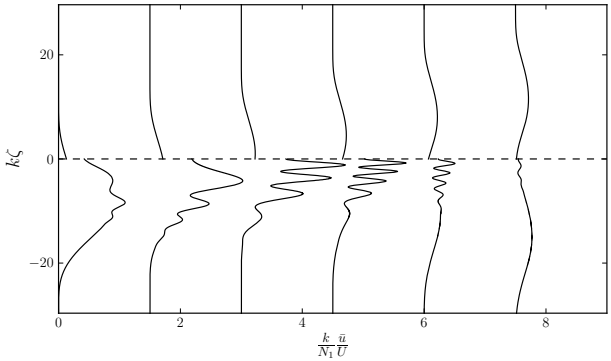

Fig. 6. Vertical profiles of the mean flow in two layers for a sequence of times. Each profile is shifted by a value of 1.5 for display. The parameter values are $n_1/k = 1/\sqrt{2}$, and $N_2/N_1 = 2$.

NPGD
1, 269–315, 2014

Incidence and reflection of internal waves

J. P. McHugh

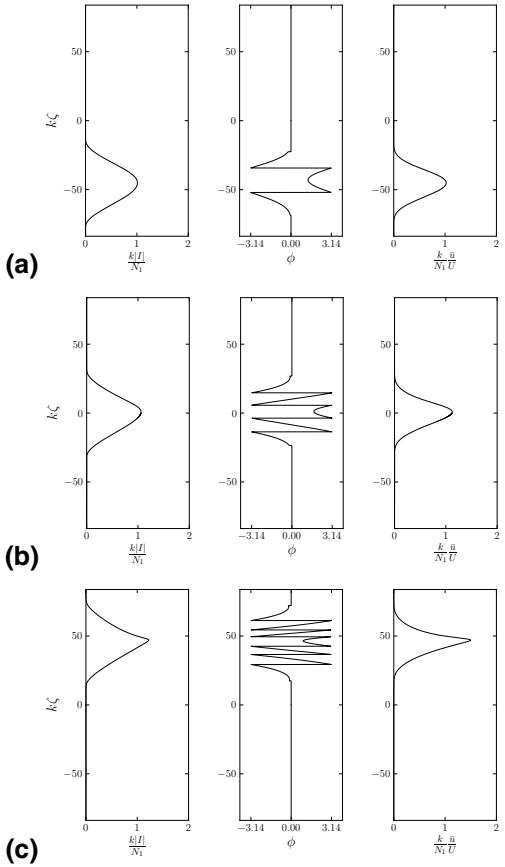

Fig. 7. Vertical profiles of the wave magnitude (left panel), phase (center panel), and mean flow (right panel) at three times in a single layer of constant N with $n_1/k = 0.4$. **(a)** $N_1\tau \approx -141$, **(b)** $N_1\tau \approx 0$, and **(c)** $N_1\tau \approx +141$.

NPGD
1, 269–315, 2014

Incidence and reflection of internal waves

J. P. McHugh

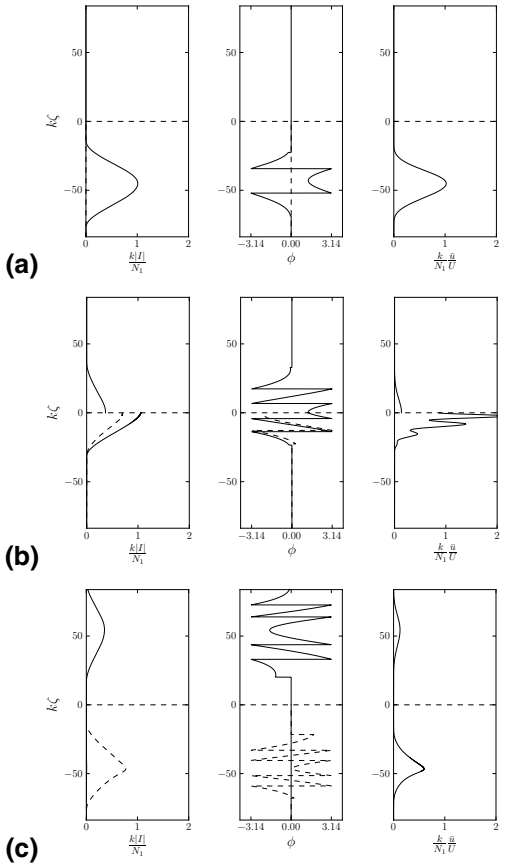

Fig. 8. Vertical profiles of the wave magnitude (left panel), phase (center panel), and mean flow (right panel) at three times in two layers. The parameter values are $n_1/k = 0.4$ and $N_2/N_1 = 2$. **(a)** $N_1\tau \approx -141$, **(b)** $N_1\tau \approx 0$, and **(c)** $N_1\tau \approx +141$.

NPGD
1, 269–315, 2014

Incidence and reflection of internal waves

J. P. McHugh

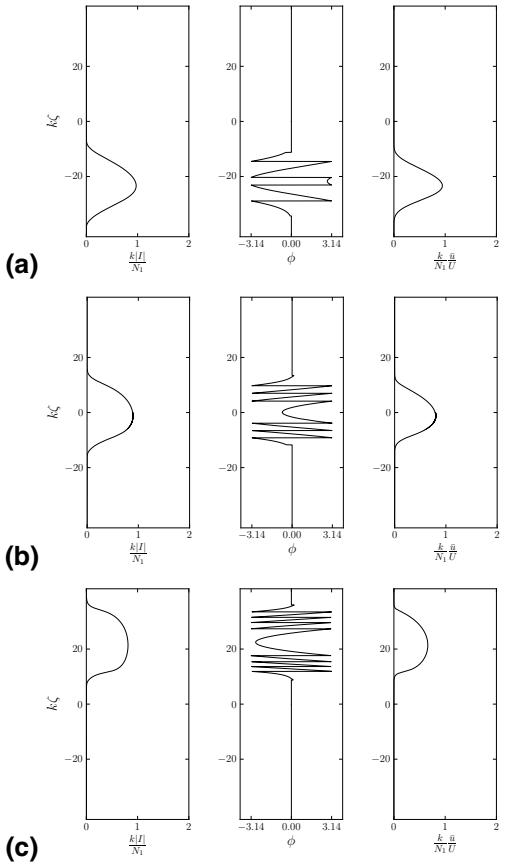

Fig. 9. Vertical profiles of the wave magnitude (left panel), phase (center panel), and mean flow (right panel) at three times in a single layer of constant N with $n_1/k = 1$. **(a)** $N_1\tau \approx -64$, **(b)** $N_1\tau \approx 0$, and **(c)** $N_1\tau \approx +64$.

NPGD
1, 269–315, 2014

Incidence and reflection of internal waves

J. P. McHugh

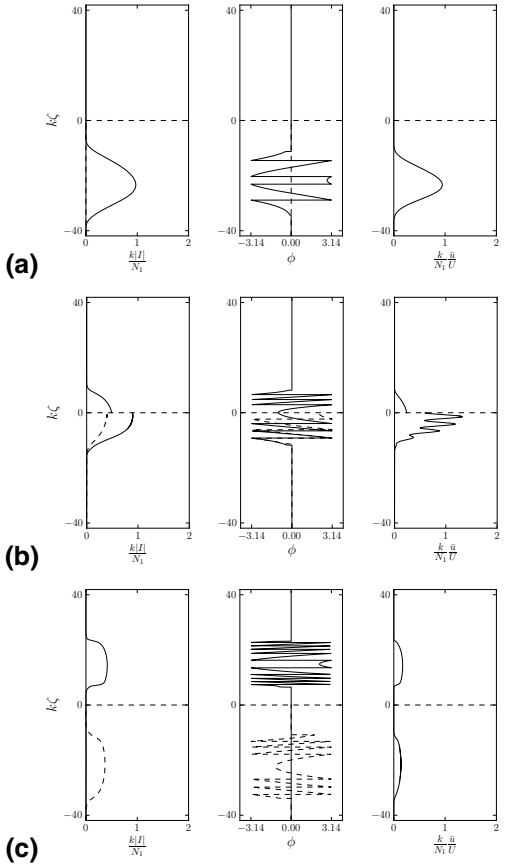

Fig. 10. Vertical profiles of the wave magnitude (left panel), phase (center panel), and mean flow (right panel) at three times in two layers. The parameter values are $n_1/k = 1$ and $N_2/N_1 = 2$. **(a)** $N_1\tau \approx -64$, **(b)** $N_1\tau \approx 0$, and **(c)** $N_1\tau \approx +64$.

NPGD
1, 269–315, 2014

Incidence and reflection of internal waves

J. P. McHugh

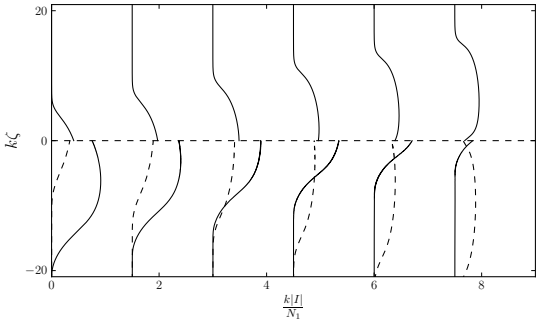

Fig. 11. Vertical profiles of the wave magnitude in two layers for a sequence of times. Each profile is shifted by a value of 1.5 for display. The parameter values are $n_1/k = 1$, and $N_2/N_1 = 2$.

NPGD
1, 269–315, 2014

Incidence and reflection of internal waves

J. P. McHugh

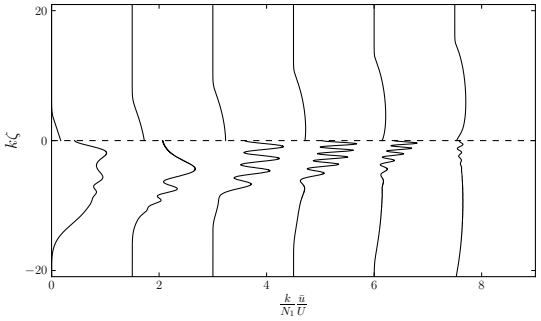

Fig. 12. Vertical profiles of the mean flow in two layers for a sequence of times. Each profile is shifted by a value of 1.5 for display. The parameter values are $n_1/k = 1$, and $N_2/N_1 = 2$.

NPGD
1, 269–315, 2014

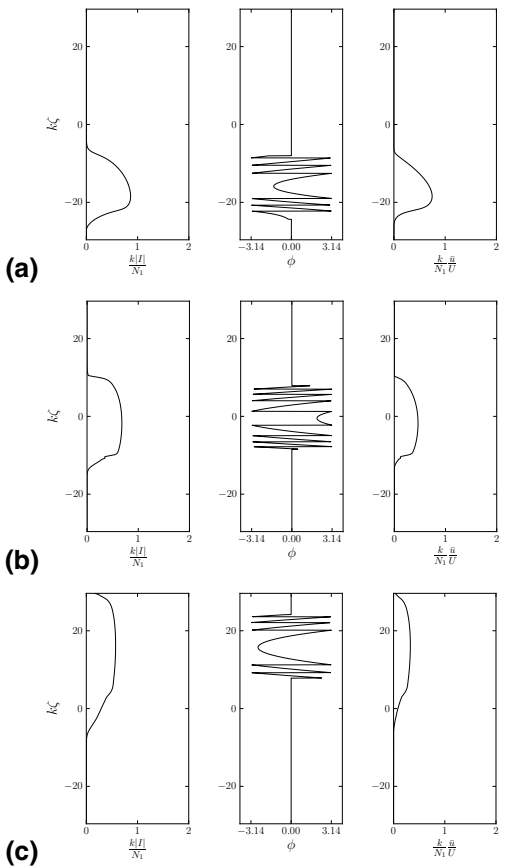

Fig. 13. Vertical profiles of the wave magnitude (left panel), phase (center panel), and mean flow (right panel) at three times in a single layer of constant N with $n_1/k = \sqrt{2}$. **(a)** $N_1\tau \approx -59$, **(b)** $N_1\tau \approx 0$, and **(c)** $N_1\tau \approx +59$.

NPGD
1, 269–315, 2014

Incidence and reflection of internal waves

J. P. McHugh

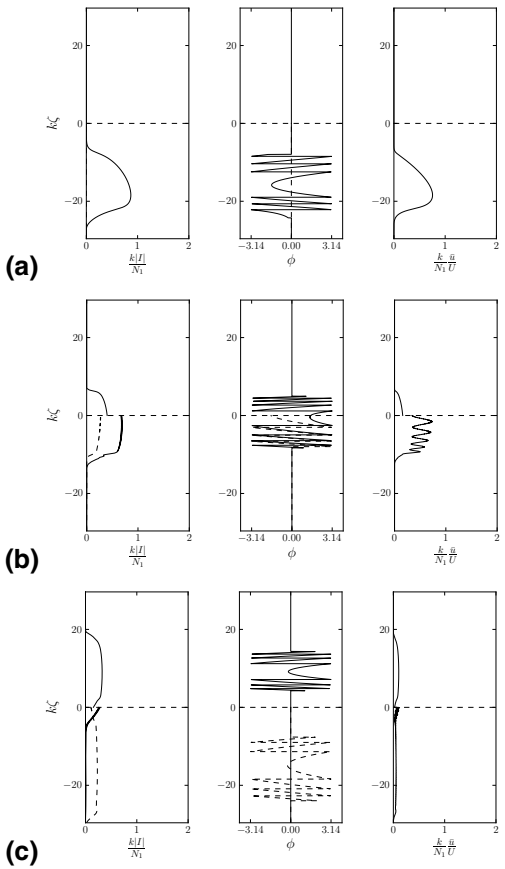

Fig. 14. Vertical profiles of the wave magnitude (left panel), phase (center panel), and mean flow (right panel) at three times in two layers. The parameter values are $n_1/k = \sqrt{2}$ and $N_2/N_1 = 2$. **(a)** $N_1\tau \approx -59$, **(b)** $N_1\tau \approx 0$, and **(c)** $N_1\tau \approx +59$.

NPGD
1, 269–315, 2014

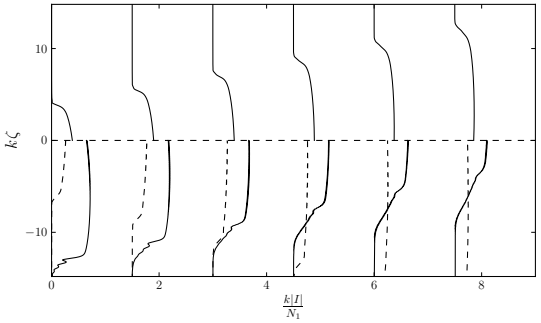

Fig. 15. Vertical profiles of the wave magnitude in two layers for a sequence of times. Each profile is shifted by a value of 1.5 for display. The parameter values are $n_1/k = \sqrt{2}$, and $N_2/N_1 = 2$.

NPGD
1, 269–315, 2014

Incidence and reflection of internal waves

J. P. McHugh

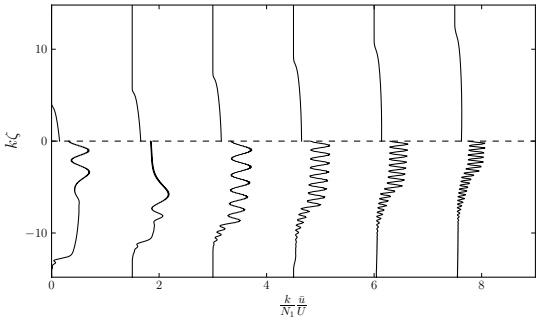

Fig. 16. Vertical profiles of the mean flow in two layers for a sequence of times. Each profile is shifted by a value of 1.5 for display. The parameter values are $n_1/k = \sqrt{2}$, and $N_2/N_1 = 2$.

NPGD
1, 269–315, 2014

Incidence and reflection of internal waves

J. P. McHugh

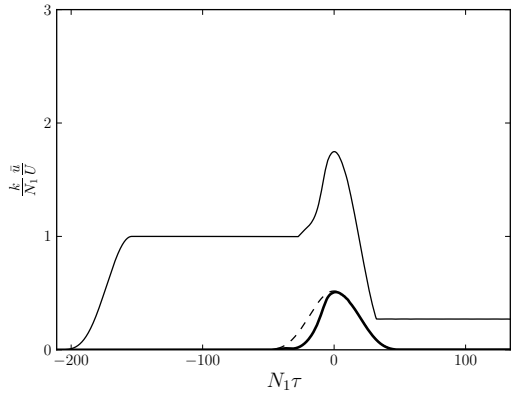

Fig. 17. Time history of the maximum of the mean flow. The dashed line is the velocity jump at the interface while the thick solid line that is the maximum the interference mean $\bar{u}_i$. The parameter values are $n_1/k = 1/\sqrt{2}$, and $N_2/N_1 = 2$.

NPGD
1, 269–315, 2014

Incidence and reflection of internal waves

J. P. McHugh

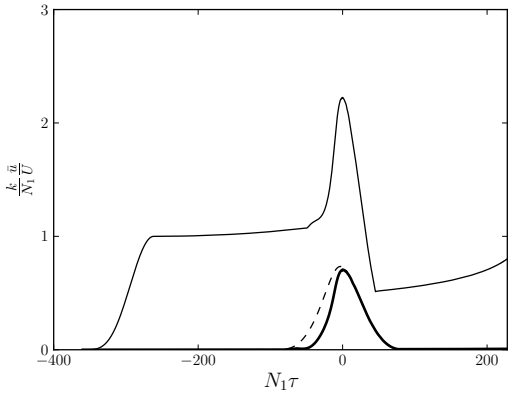

Fig. 18. Time history of the maximum of the mean flow. The dashed line is the velocity jump at the interface while the thick solid line that is the maximum the interference mean $\bar{u}_i$. The parameter values are $n_1/k = 0.4$, and $N_2/N_1 = 2$.

NPGD
1, 269–315, 2014

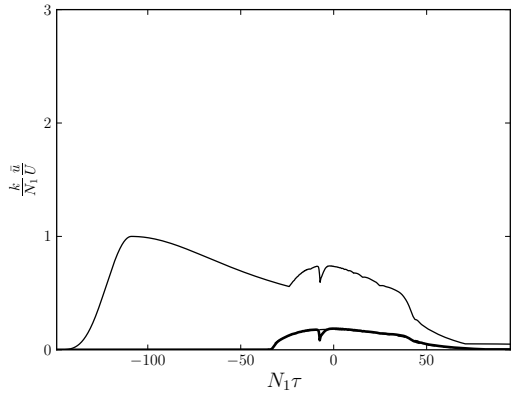

Fig. 19. Time history of the maximum of the mean flow. The dashed line is the velocity jump at the interface while the thick solid line that is the maximum the interference mean $\bar{u}_i$. The parameter values are $n_1/k = \sqrt{2}$, and $N_2/N_1 = 2$.

NPGD
1, 269–315, 2014

Incidence and reflection of internal waves

J. P. McHugh

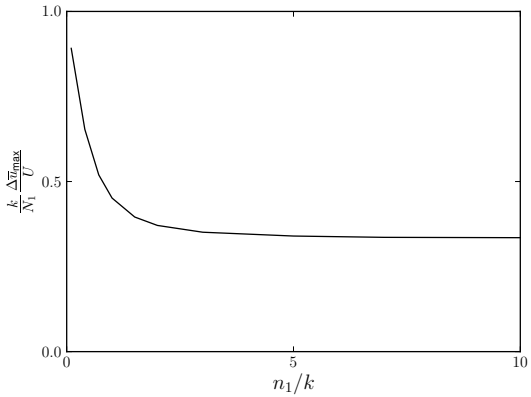

Fig. 20. The maximum of the mean velocity difference at the interface for an interval of n_1/k.

NPGD
1, 269–315, 2014

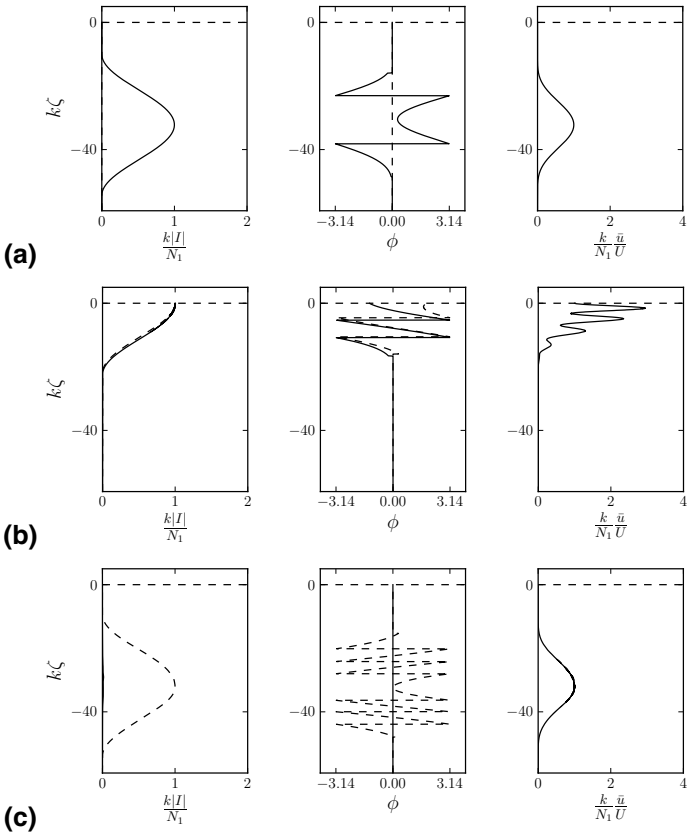

Fig. 21. Vertical profiles of the wave magnitude (left panel), phase (center panel), and mean flow (right panel) at three time values with a solid lid, with $n_1/k = 1/\sqrt{2}$. **(a)** $N_1\tau \approx -52$, **(b)** $N_1\tau \approx 0$, and **(c)** $N_1\tau \approx +52$.

NPGD
1, 269–315, 2014

Incidence and reflection of internal waves

J. P. McHugh